27 July 2022

Dropsonde Data Report

Sundowner Winds Experiment
(SWEX 2022)

Holger Vömel, Mack Goodstein, Clayton Arendt, Terry Hock, Jacquelyn Witte
Earth Observing Laboratory
National Center for Atmospheric Research
Boulder, CO

Earth Observing Laboratory
In situ Sensing Facility

NATIONAL CENTER FOR ATMOSPHERIC RESEARCH
BOULDER, COLORADO

The dropsonde data for this project were quality controlled and are maintained by the Earth Observing Laboratory at the National Center for Atmospheric Research (NCAR). The National Center for Atmospheric Research is managed by the University Corporation for Atmospheric Research and sponsored by the National Science Foundation.

If information or plots from this document are used for publication or presentation purposes, please provide appropriate acknowledgement to NCAR/EOL and NSF and refer to the citation listed below. Please feel free to contact the authors for further information.

Contact:

Holger Vömel (voemel@ucar.edu)

Dropsonde Operators:

Mack Goodstein (NCAR)
Clayton Arendt (NCAR)
Terry Hock (NCAR)

Campaign Websites:

SWEX at NCAR:
https://www.eol.ucar.edu/field_projects/swex
SWEX at U. Notre Dame:
https://efmlab.nd.edu/research/swex/
AVAPS dropsondes home page:
https://www.eol.ucar.edu/observing_facilities/avaps-dropsonde-system

To refer to this data set or report, please include the following citation:

NCAR/EOL Dropsonde Team. 2022. SWEX: NCAR/EOL AVAPS Dropsonde Profiles. Version 1.0. UCAR/NCAR - Earth Observing Laboratory. https://doi.org/10.26023/AGME-MF19-NJ0A. Accessed 27 Jul 2022.

Cover photo: Clayton Arendt in front of the NPS Twin Otter. Photo by Terry Hock

Document Version Control

Version	Date	Author	Change Description
1.0	26 July 2022	H. Vömel	Initial release

Table of Contents

1 Dataset overview

The Sundowner Winds Experiment (SWEX) studies the meteorological processes that control the downslope windstorms at the lee of the Santa Ynez Mountains in Santa Barbara County. These windstorms known as Sundowner winds are one of the most significant fire weather hazards affecting populated areas. They typically peak from early evening to mid-morning and modeling results show that the intensity and spatial variation of Sundowners are driven by a combination of dynamic and thermodynamic mechanisms that depend on the complex-terrain boundary layer dynamics, profiles of winds and stability.

The main goal of this study is to improve the current understanding of the dynamics and predictability of downslope windstorms in coastal Santa Barbara County. This project studies how the boundary layer structure and dynamics spanning the Santa Ynez Mountains and Santa Ynez Valley influence Sundowner winds intensity, timing and geographic characteristics. It examines mechanisms relating high amplitude mountain waves, critical layers, and surface wind intensity, and how variations in boundary layer structure and tropospheric stability influence the predictability of Sundowner winds.

In addition to numerous surface observations, the campaign used an instrumented research aircraft to conduct airborne operations covering the Santa Ynez Mountains and coastal area just south of Santa Barbara County. One of the important datasets for this field campaign is the thermodynamic structure of the atmosphere measured by dropsondes released from the Naval Postgraduate School (NPS) Twin Otter research aircraft, which was stationed at Oxnard, CA, for the duration of the campaign. Between 4 April and 15 May 2022, 159 dropsondes were released from twenty research flights and targeted the boundary layer to the north and south of the Santa Ynez Mountains. Soundings were typically released from an altitude of 3.5 km. All soundings provided complete profiles of all parameters with a nominal vertical resolution between 5 to 6 m from the surface to almost flight altitude. SWEX deployed the NRD41 dropsonde, which is the most advanced model that has been developed at NCAR.

All flight tracks and all dropsonde release locations are shown in Figure 1. All dropsondes were released at predetermined locations and tracked to the surface.

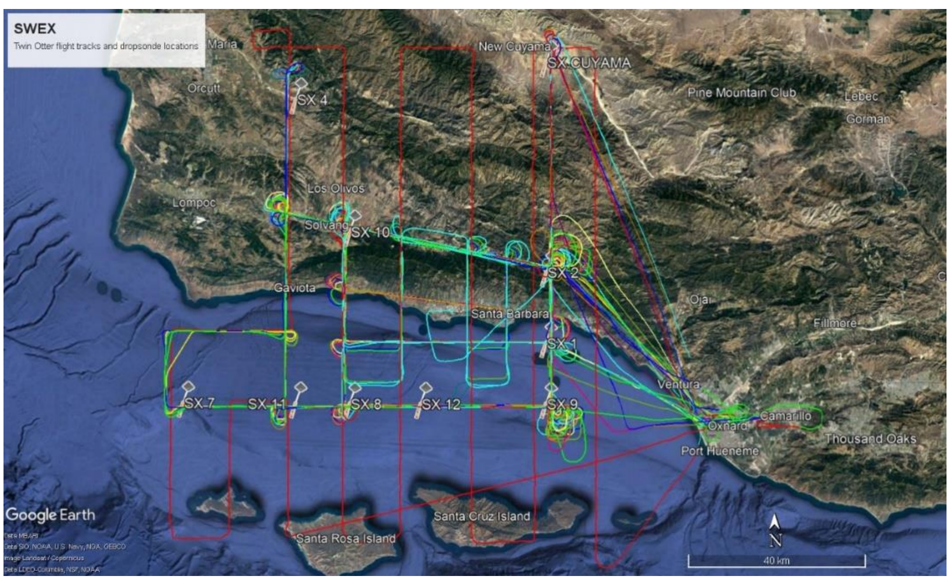

Figure 1: Flight tracks of all research flights that released dropsondes during SWEX. Dropsonde icons indicate waypoints at which dropsondes were launched.

Table 1 provides an overview over all NCAR NRD41 dropsondes released during SWEX. Between four and ten sondes were launched on each research flight. All dropsonde releases are listed in Appendix A. On almost all flight days, two flights were conducted, one in the afternoon, and a second in the evening with a roughly 2 hour refueling stop at Oxnard.

Table 1: Overview over all flights releasing dropsondes during SWEX.

Research Flight	Date	# of Sondes
RF01	04 Apr	5
RF02	05 Apr	8
RF03	06 Apr	4
RF03b	06 Apr	5
RF04	13 Apr	5
RF05	14 Apr	8
RF06	17 Apr	5
RF07	18 Apr	8
RF08	18 Apr	5
RF09	19 Apr	9
RF10	23 Apr	7
RF11	24 Apr	8
RF12	25 Apr	6
RF13	26 Apr	9
RF14	28 Apr	6
RF15	29 Apr	8
RF16	04 May	6
RF17	05 May	9
RF18	08 May	7
RF19	08 May	7
RF20	09 May	9
RF21	10 May	5
RF22	11 May	10

Drops were scheduled over pre-determined waypoints, which are indicated in Figure 1 and listed in Table 2. The single sonde released at waypoint SX 10 was unscheduled to make up for the missed launch at SX 2.

Waypoint	Longitude	Latitude	# of Sondes	Type
SX CUYAMA	-119.61	34.92	6	Land drop
SX 4	-120.21	34.85	8	Land drop
SX 10	-120.08	34.59	1	Land drop
SX 2	-119.61	34.51	47	Land drop
SX 1	-119.61	34.37	4	Ocean drop
SX 9	-119.61	34.25	34	Ocean drop
SX 12	-119.91	34.25	19	Ocean drop
SX 8	-120.08	34.25	11	Ocean drop
SX 11	-120.21	34.25	20	Ocean drop
SX 7	-120.48	34.25	9	Ocean drop

Table 2: Flight track waypoints at which dropsondes were released. Waypoints are sorted from North to South. Sixty-two sondes were dropped over land, 97 sondes were dropped over the ocean.

Table 3 provides an overview of the performance of the dropsonde system as a whole. In total, 159 sondes were released from the aircraft. All sondes released but one reported complete atmospheric profiles to the ground.

The overall success rate of the dropsonde system for this campaign is at 99%.

Table 3: Overview of the dropsonde system performance.

	# of Sondes	Percent
Total number of sondes released	159	100
Successful releases	159	100
Complete thermodynamic profiles to the ground	158	99
Complete wind profiles to the ground	158	99

2 Dropsonde sounding system

For SWEX, an NCAR 8-channel AVAPS® dropsonde system was installed aboard the Naval Postgraduate School (NPS) Twin Otter research aircraft using an open dropsonde launch tube for the NCAR Research Dropsonde model NRD41.

This dropsonde uses the pressure, temperature, and humidity sensor of the Vaisala RS41 radiosonde and employs an improved version of the GPS receiver, telemetry, and parachute release system of the previous NRD94 dropsonde, which had been in use between 2011 and 2018. It has been successfully deployed during several previous field campaigns including the Organization of Tropical East Pacific Convection (OTREC) field campaign in August and September of 2019 (Vömel et al, 2021) and the Chemistry in the Arctic: Clouds, Halogens, and Aerosols CHACHA in March and April 2022. Twenty-eight of the NRD41 dropsondes were equipped with an infrared sensor to measure the sea surface temperature. These observations were experimental to evaluate the accuracy of this sensor.

All dropsonde humidity sensors were reconditioned prior to launch. This process, which is unique to the xRD41 dropsondes, reduces the potential of humidity contamination to a minimum and assures the best measurement performance throughout the entire altitude and temperature range of the profiles.

The AVAPS LabVIEW based software system receives and stores data from the dropsondes, and the AVAPS receiving system, including a reference GPS receiver. The AVAPS Control Software (ACS) was operated in parallel for evaluation of this new software. All data reported here were recorded using the AVAPS LabVIEW based software.

The dropsonde operator onboard the NPS Twin Otter research aircraft released all dropsondes through an open dropsonde launch tube, which was installed towards the aft of the aircraft. GNSS signals within the cabin assured that all dropsondes tracked GPS satellites signals at the time of launch. There was no aircraft data system/sensors to provide atmospheric conditions at flight level to initialize each drop.

Profile data were collected after the completion of each research flight and transferred to the SWEX field catalog, which was maintained by NCAR/EOL. Data were not transmitted to the Global Telecommunications System (GTS) of the WMO.

3 Quality control procedures

3.1 Standard quality control

Standard quality control in near real time and as part of the final data QC is based on the algorithms implemented in the ASPEN software. The following quality checks, corrections, and calculations are performed:

- Removal of outliers and suspect data points in pressure, temperature, humidity, zonal and meridional wind, latitude, and longitude
- Removal of data between release from the aircraft and equilibration with atmospheric conditions
- Dynamic correction to account for the lag of the NRD41 temperature sensor using the appropriate coefficients for the NRD41 dropsondes
- Dynamic correction to account for the sonde inertia in the determination of the wind profile using the appropriate parameters for the NRD41 dropsondes
- Smoothing of pressure, temperature, humidity, zonal and meridional wind
- Recomputing of wind speed and wind direction after smoothing of the wind components
- Extrapolation of the last reported pressure reading to a surface pressure value (where possible), based on the fall rate of the sonde
- Recalculation of the geopotential height from the surface to the top of the profile
- Computing a vertical wind speed component

This campaign used the NRD41 dropsonde, which has a faster temperature sensor and faster RH sensor than the older NRD94 sondes. This has been considered in the final dropsonde QC by changing the ASPEN QC parameters for these two sensors. The equilibration time for the temperature and RH sensor has been adjusted to 5 s, and the smoothing wavelength for both parameters has been adjusted to 5 s.

3.2 Custom quality control

3.2.1 Winds

The GPS receiver in the dropsondes operated properly in all but five soundings, i.e. the reported speed uncertainty of the GPS was around its nominal value of 0.2 m/s. In four of these soundings, the speed uncertainty was slightly degraded to values around 0.6 m/s, with otherwise normal GPS performance. Sounding 20220505_033833 lost GPS tracking at launch and regained tracking at 1.8 km.

Table 4: Soundings with degraded GPS tracking.

Research Flight	Sounding
RF02	20220405_004532
RF03b	20220406_072714
RF05	20220414_025633
RF15	20220429_044856
RF17	20220505_033833

3.2.2 Pressure

The pressure sensor of the NRD41 dropsonde is known to have a small bias. This sensor bias is measured during the production of the dropsondes and a correction is stored in the sonde to minimize the bias during observation.

The statistics of the pressure bias measured and corrected during production is shown in Figure 2. The median pressure correction is -1.30 hPa and the standard deviation 0.26 hPa. These measurements were used to correct the dropsonde pressure readings during production. Some drift between production and use of the sonde is possible, but still, the surface pressures reported by the dropsondes are expected to have only small systematic biases. The pressure inside the cabin or the launch tube was not measured and the pressure measurements of the dropsondes prior to launch could not be validated.

Sonde 20220429_030022 and 20220508_023019 did not use a production pressure correction. The pressure readings of this sounding may be low biased by up to 1.5 hPa.

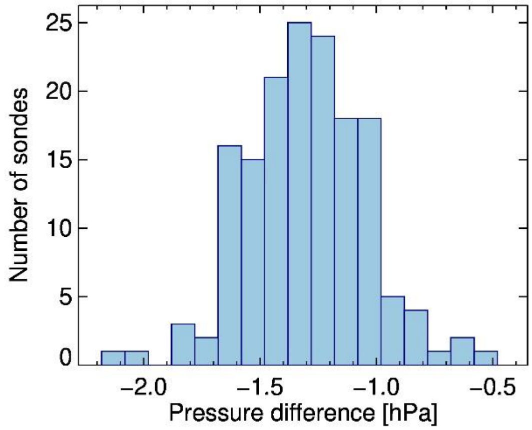

Figure 2: Pressure offset between the dropsonde and the reference sensor before launch.

The pressure sensor in sonde 20220404_213400 showed unusually large noise. For this sounding, the pressure was calculated from the GPS altitude and initialized by the surface pressure. For this sounding, 10 s of data after launch were removed, where the pressure calculated from GPS showed larger than expected errors.

During SWEX, most sondes exhibited a small pressure measurement issue. For reasons currently unknown, the dropsondes occasionally repeated a reported pressure measurement. This happened up to 19 times per sounding. While this is barely noticeable in any vertical profile, it did lead to additional noise in the calculated vertical fall rate. In post processing, these repeated pressure readings were interpolated and the fall rates were recalculated excluding these values. Only pressure readings had to be corrected. Temperature and relative humidity readings did not show any artificial repetition of measurements.

3.2.3 Relative humidity

The RH sensor on the xRD41 dropsondes should be reconditioned prior to launch. The sondes store the information, whether the reconditioning was successful, and we were able to verify that all sondes were properly reconditioned prior to take off before each flight. Any contamination in the sensor material was removed and the relative humidity sensors were expected to perform with negligible calibration drift. During SWEX all dropsondes were properly reconditioned and no bias is relative humidity measurements is expected.

The time response of the NRD41 relative humidity sensor is a less than one seconds near the surface and up to 4 s at flight level of the NPS Twin Otter. The effect of the time humidity sensor time lag correction is small for the observations during SWEX and no correction was not applied in post processing.

We removed the first 5 s of the relative humidity and temperature profiles, while the sensors are equilibrating to the ambient environment. Since the sensor temperature changes from the warm cabin air to colder ambient air, equilibration of the humidity sensor is faster than it would be at the colder ambient conditions in steady state.

3.3 Sonde tracking

For sondes dropped over land, every attempt was made to track the telemetry signal all the way to the ground. Most sondes reported data from the surface, which allowed evaluating to what altitude telemetry was tracked. In only three soundings the telemetry signal could not be tracked to the ground due to shadowing of a nearby ridge. For these soundings, the surface elevation was determined from the location were the sonde landed. Shadowing due to a mountain ridge caused a loss of telemetry signal of at most 30 m.

Table 5: Telemetry loss due to mountain shadowing

Research Flight	Sounding	Landing elevation [m]	Altitude of last telemetry signal [m]
RF01	20220426_054804	501	521
RF03	20220505_043208	456	485
RF03b	20220504_225107	460	489

The telemetry of sounding 20220429_030022 was lost at 809 m above the ocean due to operator error. About 350 m of data could be recovered from data recorded in parallel by the new ACS software; however, no data are available below 458 m above the ocean surface.

4 Data file format

The format follows that defined for the NCAR/EOL/ISF radiosonde NetCDF data files. It is based on the Climate and Forecasting (CF) convention version 1.6 and is compatible with any tool accepting this convention. The data file format is described in Vömel et al. (2019).

5 Sounding metrics

5.1 Surface pressure

The surface pressure reported by the sondes is an extrapolation of the last measured air pressure down to the surface using the current fall rate. For sondes over the ocean, the sea level pressure is shown in Figure 3 as a sequence of soundings and not as a function of time.

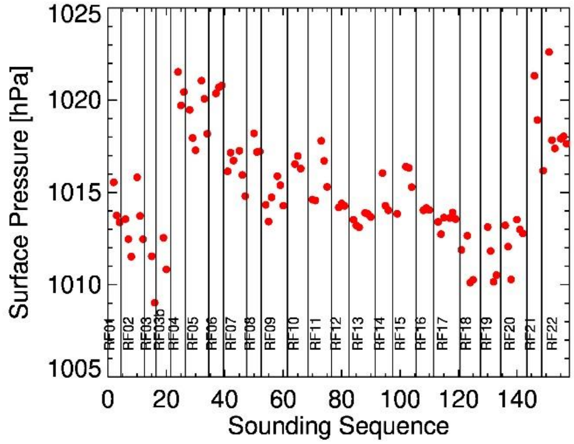

Figure 3: Sea surface pressure reported by all sondes launched over the ocean.

5.2 Fall rate

A histogram of the fall speed near the surface is shown in Figure 4. All parachutes functioned as expected. The fall time varied from 4.1 min during the early phase of the campaign to 5.5 min during the later phase when sondes were dropped from a higher altitude. All parachutes inflated within seconds after launch.

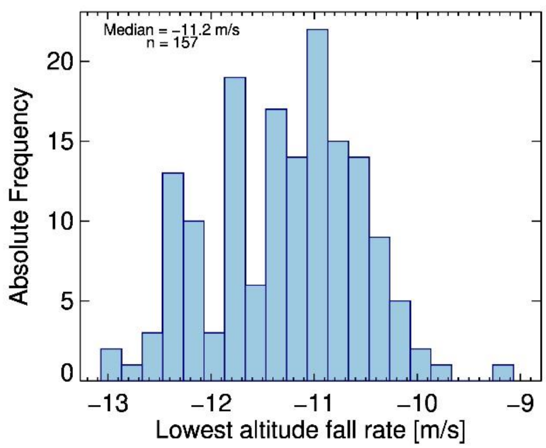

Figure 4: Distribution of the fall speed near the surface for all soundings.

5.3 Horizontal drift

Wind speeds during SWEX were on average about 10 m/s and did not exceed 28 m/s in any sounding in the altitude range below the aircraft. On average sondes traveled 2.2 km, with a maximum of 5.4 km. (Figure 5). For dropsonde releases in stronger winds over the mountains, the aircraft crew adjusted the flight track at drop location SX 2 slightly to avoid landing dropsondes on top of the mountain range, which happened in 4 soundings during the first 3 research flights (

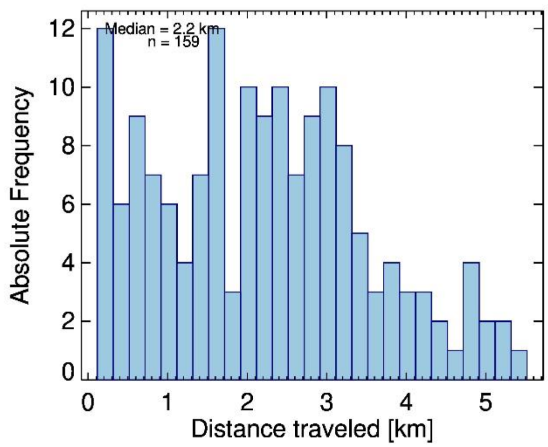

Figure 5: Distance between launch and landing for all dropsondes during SWEX.

).

Research Flight	Sounding	Landing elevation
RF01	20220404_204346	844
RF02	20220405_004532	995
RF03	20220406_023043	963
RF03b	20220406_063210	957

Table 6: Dropsonde launches with landing elevations above 800 m.

6 Observations

6.1 Temperature

The temperature measured by all dropsondes is shown as a contour plot in Figure 6. Individual research flights are separated by vertical lines and contain between four and ten dropsonde launches. Temperatures at flight level were in the range of -10°C to +12°C and near the surface in the range of 10°C to 24°C over the ocean and up to 26°C over land.

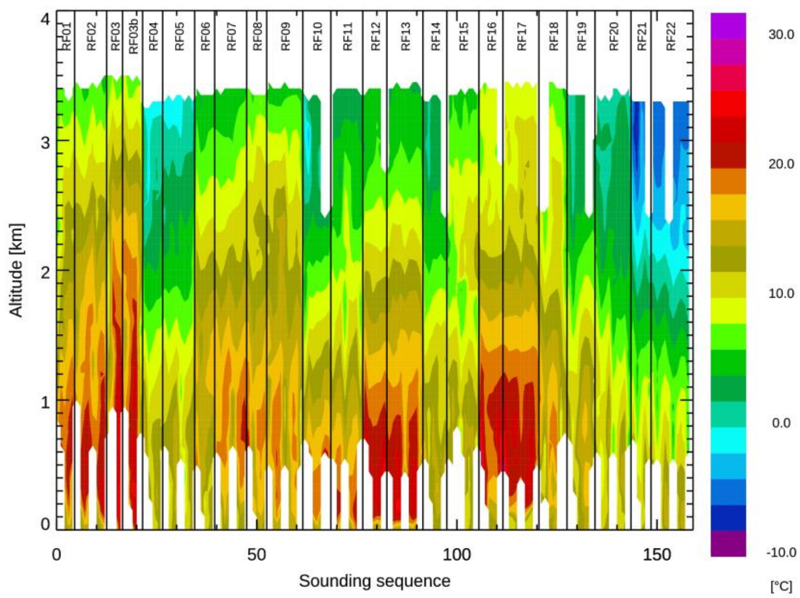

Figure 6: Color contours for all temperature measurements. All soundings are shown in the sequence in which they were released. The research flights are indicated near the top.

6.2 Relative humidity

Relative humidity reported by all dropsondes is shown in Figure 7. All dropsonde profiles were largely above 0°C and very few soundings were dropped through clouds. Sounding 20220423_221328 showed saturation at an altitude of 3 km, about 350 m below flight level, and the ocean soundings during RF17 on 4 May (5 May UTC) show near saturation in the lowest 50 m of their profiles.

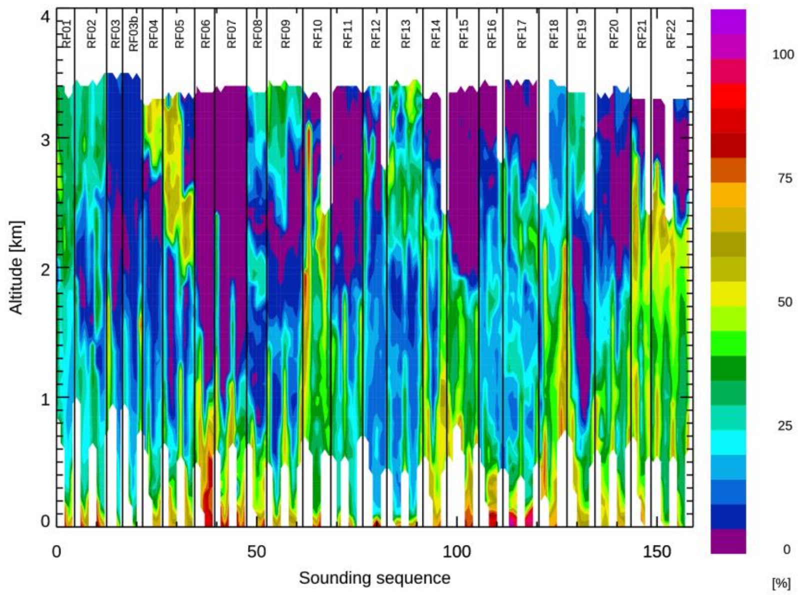

Figure 7: Color contours for relative humidity.

6.3 Winds

Zonal and meridional wind speeds are shown in Figure 8. These plots allow identification of the different general wind structure observed during each research flight.

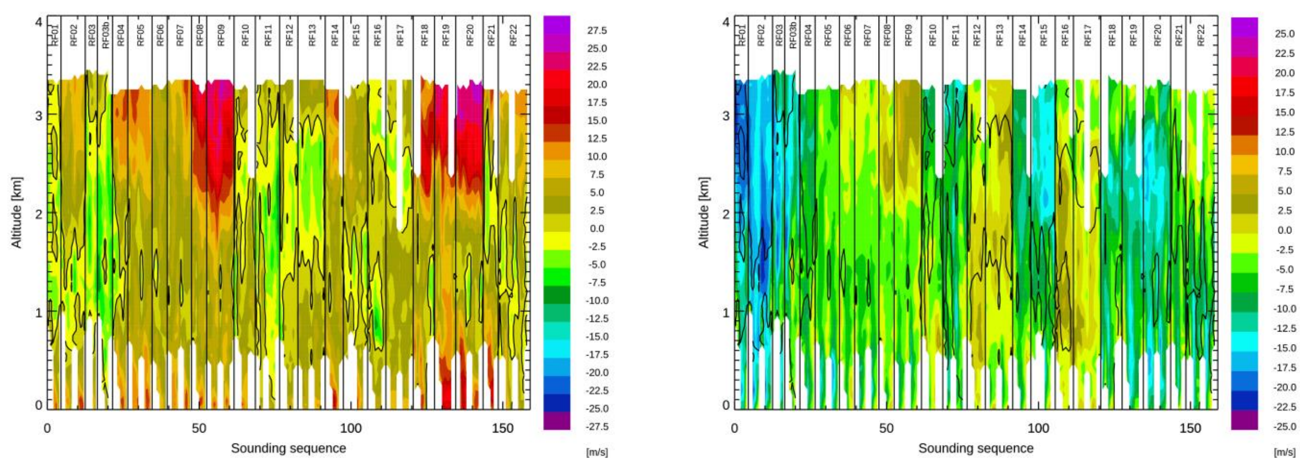

Figure 8: Color contours for all zonal (left) and meridional (right) wind speed measurements. Brown and red colors indicate westerly/southerly winds, green and blue colors indicate easterly/northerly winds.

The wind speeds for all profiles are shown in Figure 9. The average for all profiles shows the lowest average wind speeds between 600 and 1600 m height. Wind speeds are increasing above and below. This characteristic wind profile structure is due to the sampling bias during SWEX, which targeted sundowner events.

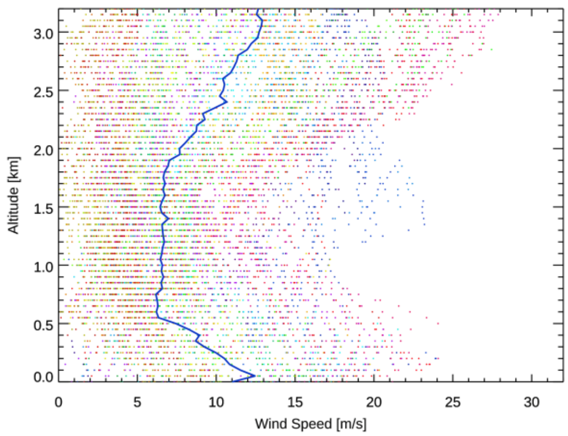

Figure 9: Wind speed for all dropsondes during SWEX. Data points of the same color belong to the same drop. The solid blue line is the mean of all profiles at each altitude.

6.4 Vertical winds

Dropsondes can sense stronger vertical winds, which are calculated as the difference between the theoretical and the measured fall rates (Wang et al., 2008). Many soundings showed significant updrafts and downdrafts (Figure 10), indicating some turbulence, which was on occasion observed by the aircraft as well.

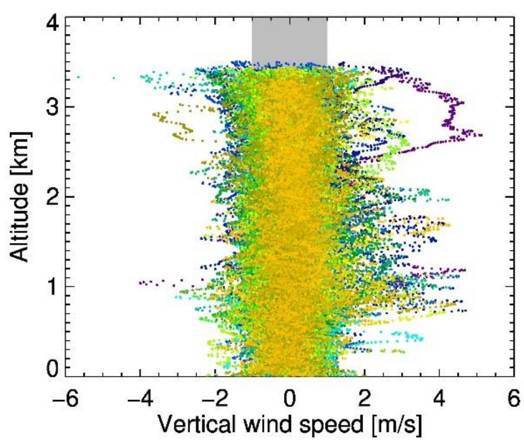

Figure 10: Vertical wind speeds for all soundings derived from the measured fall rate. The grey shaded area indicates the estimated uncertainty for vertical winds derived by this method. Data points of the same color belong to the same drop.

6.5 Summary plots

Flights using dropsondes targeted meteorological conditions conducive for Sundowner events. All profiles are shown below. All profiles but one ending at an altitude higher than 0 m were launched over land and were tracked to the surface.

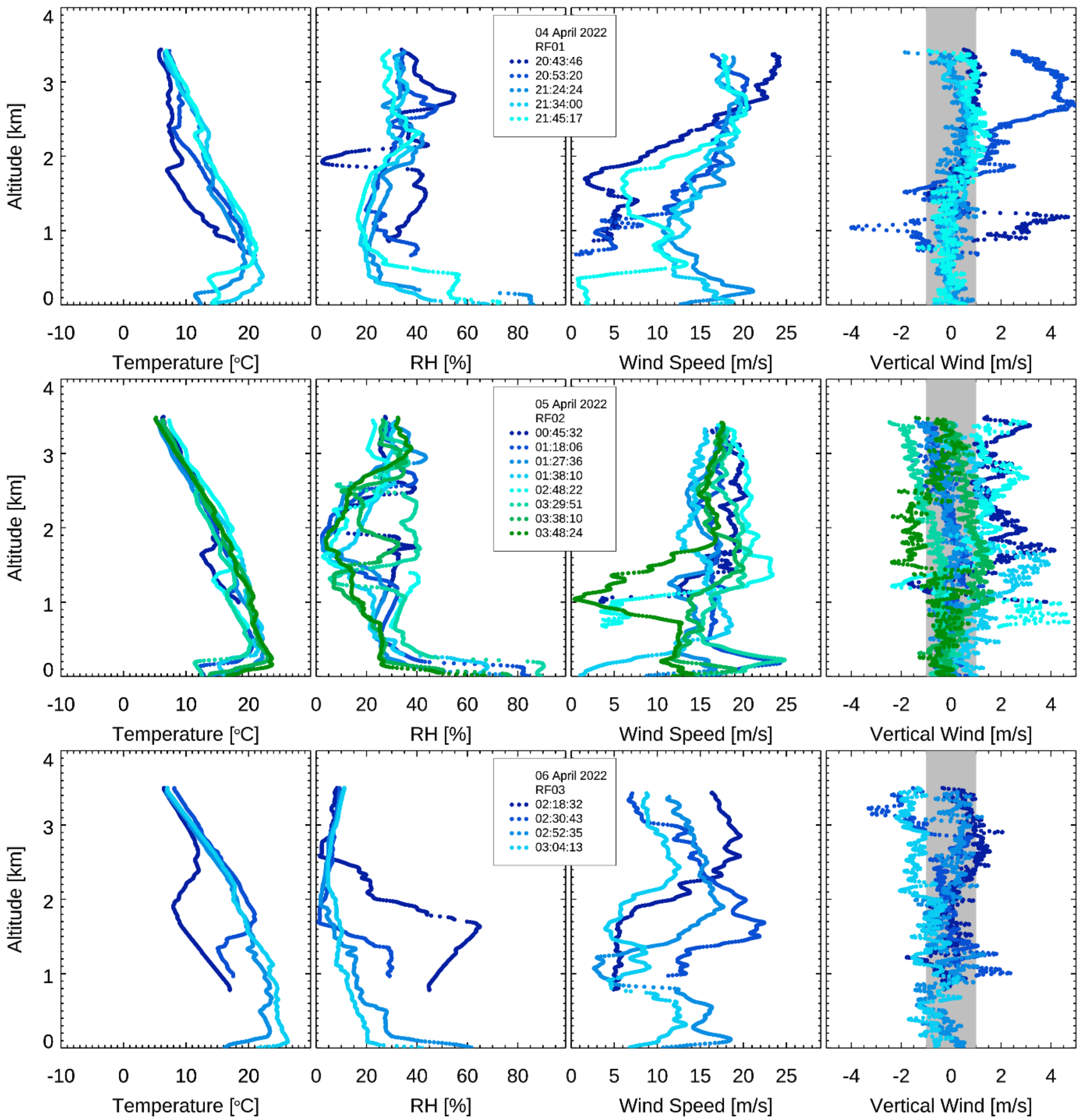

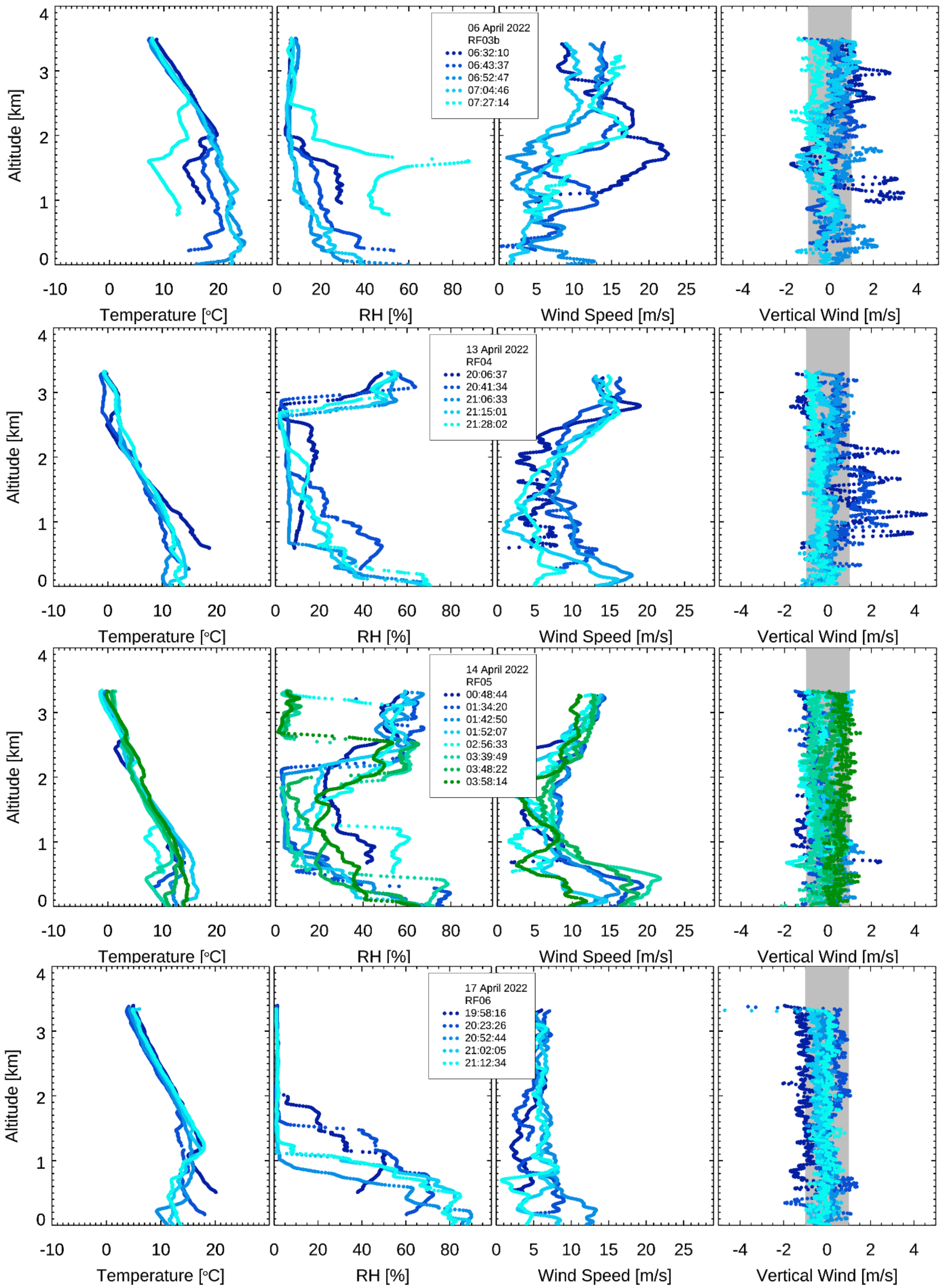
Altitude [km]
Temperature [°C]
RH [%]
Wind Speed [m/s]
Vertical Wind [m/s]
06 April 2022
RF03b
06:32:10
06:43:37
06:52:47
07:04:46
07:27:14
13 April 2022
RF04
20:06:37
20:41:34
21:06:33
21:15:01
21:28:02
14 April 2022
RF05
00:48:44
01:34:20
01:42:50
01:52:07
02:56:33
03:39:49
03:48:22
03:58:14
17 April 2022
RF06
19:58:16
20:23:26
20:52:44
21:02:05
21:12:34

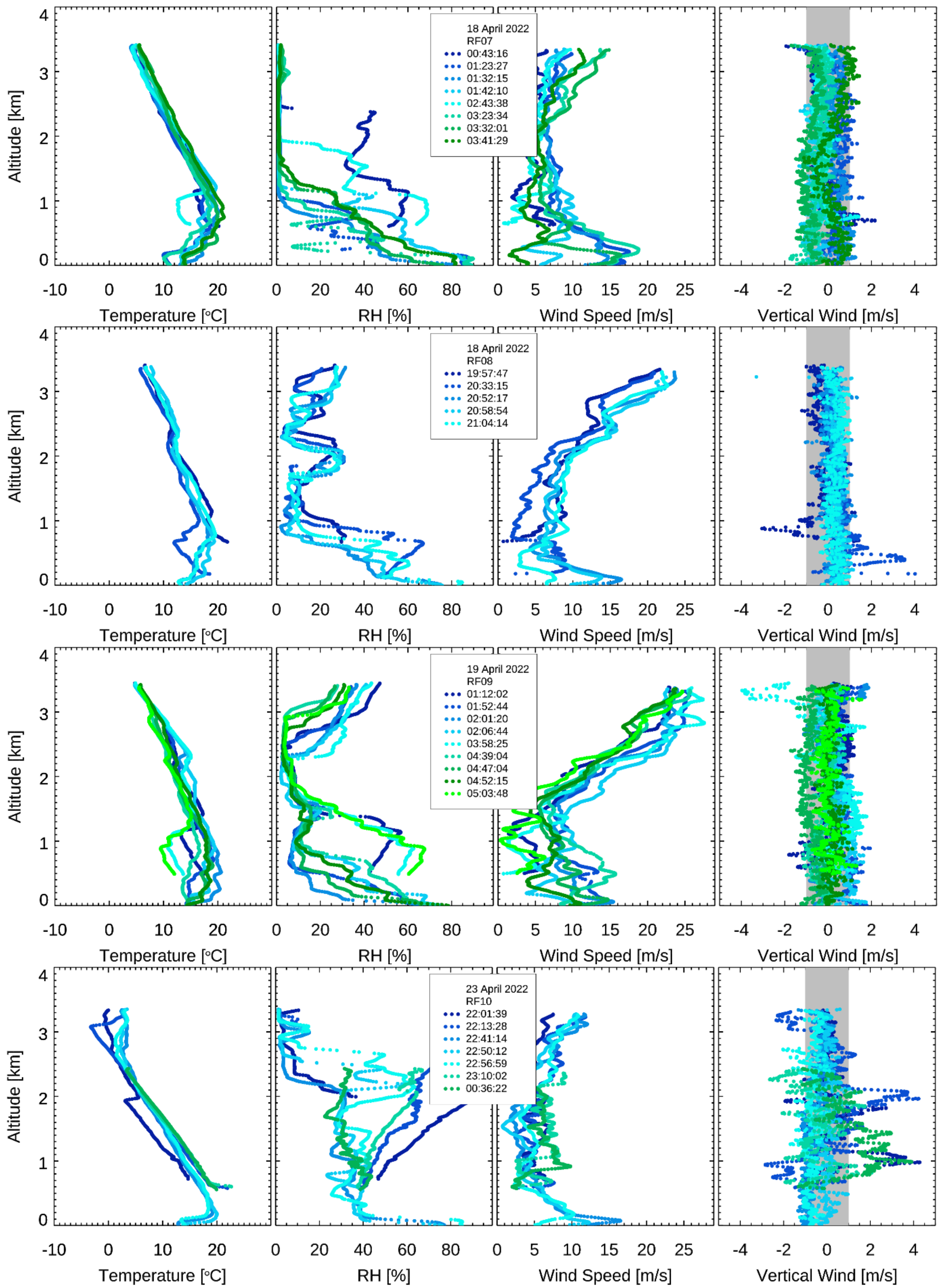

18 April 2022
RF07
00:43:16
01:23:27
01:32:15
01:42:10
02:43:38
03:23:34
03:32:01
03:41:29
18 April 2022
RF08
19:57:47
20:33:15
20:52:17
20:58:54
21:04:14
19 April 2022
RF09
01:12:02
01:52:44
02:01:20
02:06:44
03:58:25
04:39:04
04:47:04
04:52:15
05:03:48
23 April 2022
RF10
22:01:39
22:13:28
22:41:14
22:50:12
22:56:59
23:10:02
00:36:22
Altitude [km]
Temperature [°C]
RH [%]
Wind Speed [m/s]
Vertical Wind [m/s]

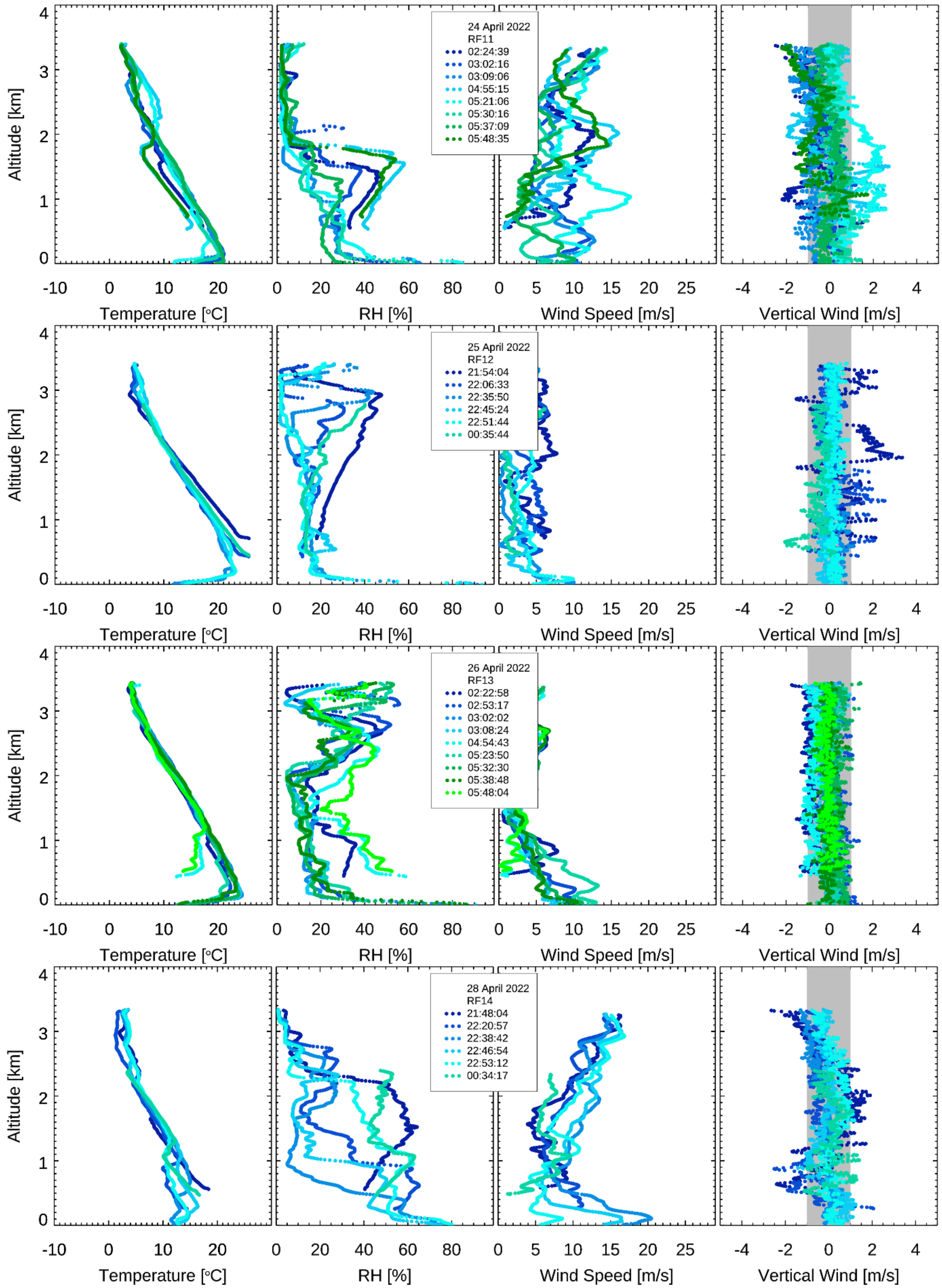
24 April 2022
RF11
02:24:39
03:02:16
03:09:06
04:55:15
05:21:06
05:30:16
05:37:09
05:48:35
25 April 2022
RF12
21:54:04
22:06:33
22:35:50
22:45:24
22:51:44
00:35:44
26 April 2022
RF13
02:22:58
02:53:17
03:02:02
03:08:24
04:54:43
05:23:50
05:32:30
05:38:48
05:48:04
28 April 2022
RF14
21:48:04
22:20:57
22:38:42
22:46:54
22:53:12
00:34:17
Altitude [km]
Temperature [°C]
RH [%]
Wind Speed [m/s]
Vertical Wind [m/s]

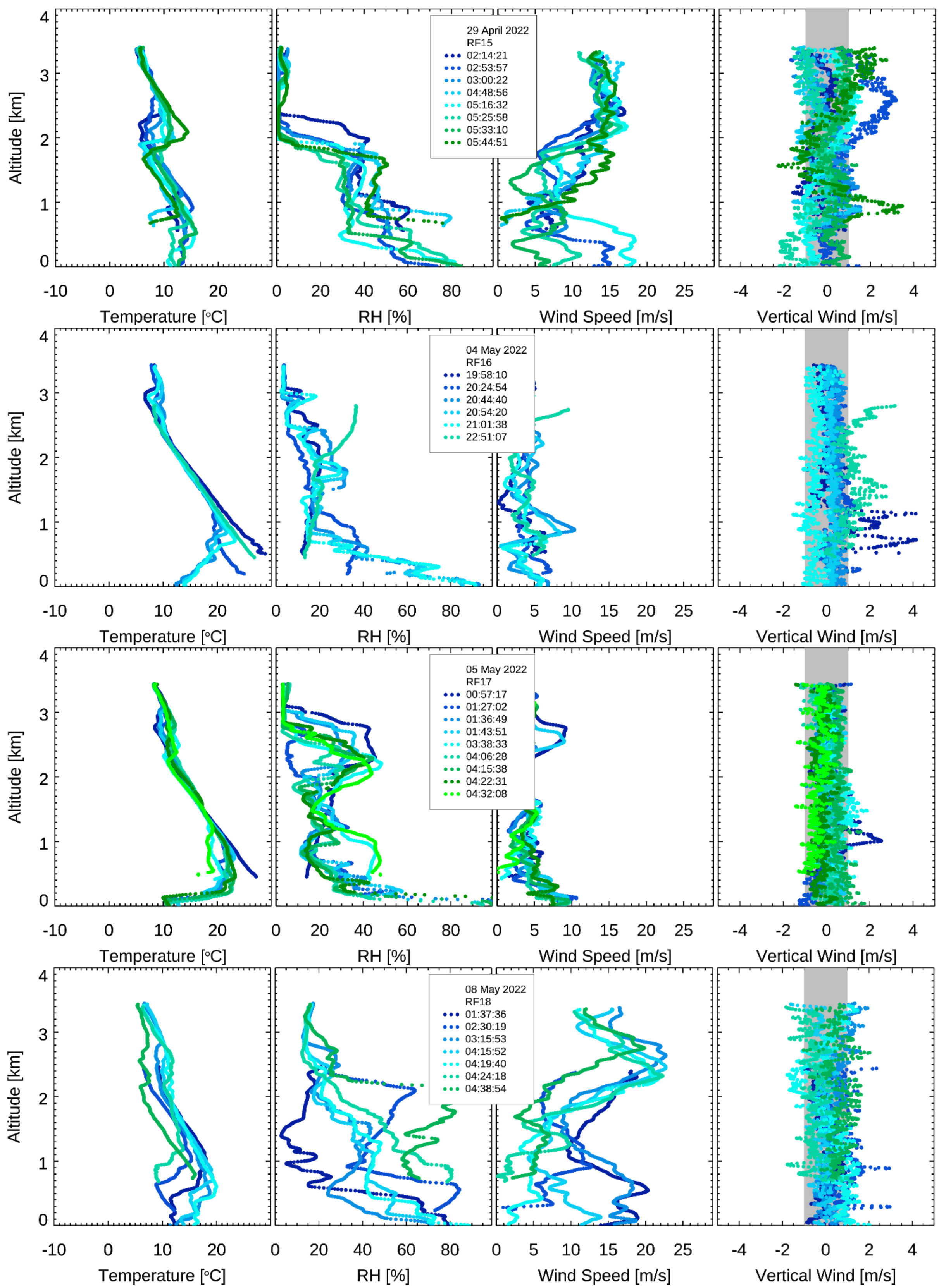
29 April 2022
RF15
02:14:21
02:53:57
03:00:22
04:48:56
05:16:32
05:25:58
05:33:10
05:44:51
04 May 2022
RF16
19:58:10
20:24:54
20:44:40
20:54:20
21:01:38
22:51:07
05 May 2022
RF17
00:57:17
01:27:02
01:36:49
01:43:51
03:38:33
04:06:28
04:15:38
04:22:31
04:32:08
08 May 2022
RF18
01:37:36
02:30:19
03:15:53
04:15:52
04:19:40
04:24:18
04:38:54
Altitude [km]
Temperature [°C]
RH [%]
Wind Speed [m/s]
Vertical Wind [m/s]

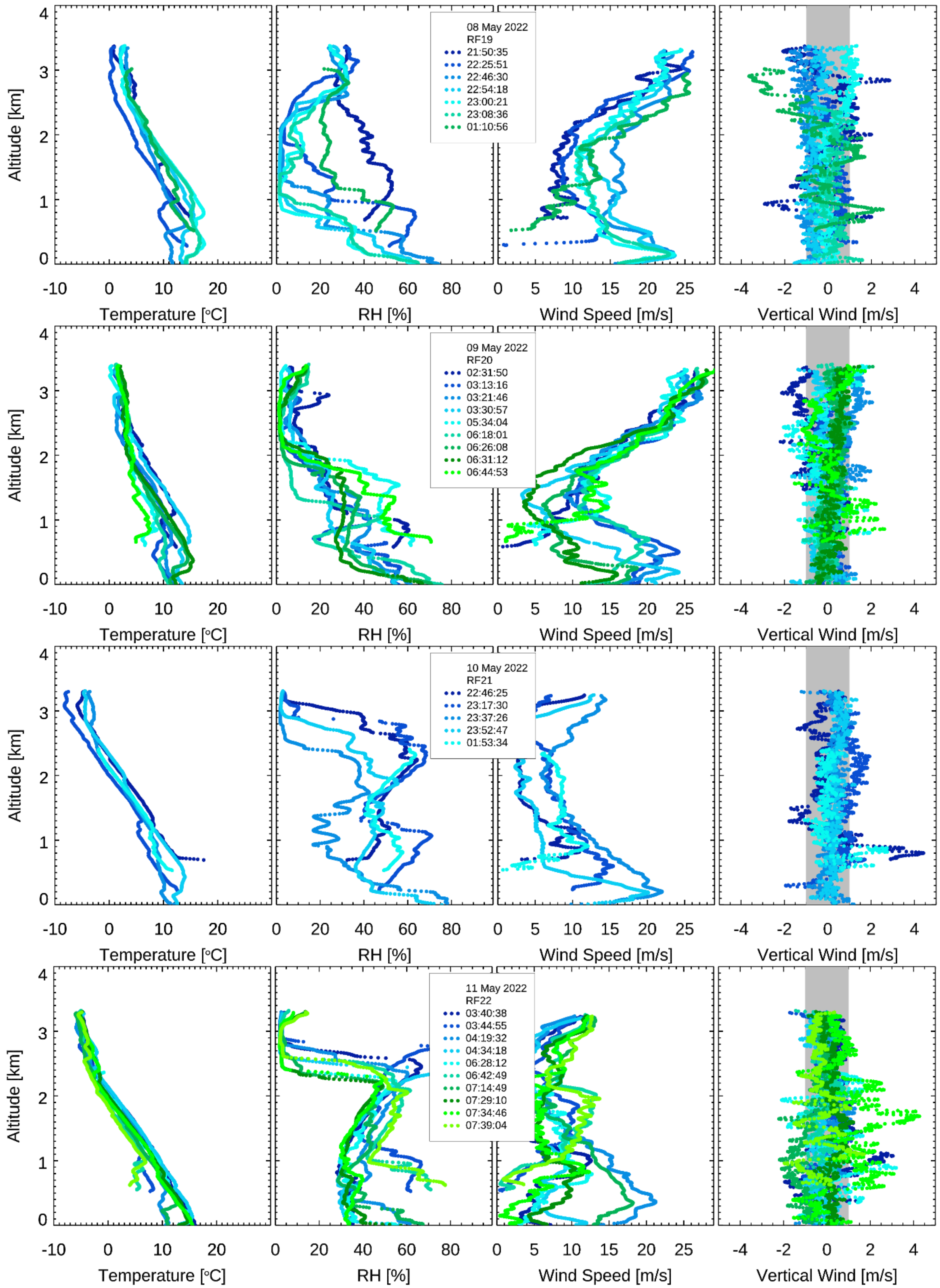
08 May 2022
RF19
21:50:35
22:25:51
22:46:30
22:54:18
23:00:21
23:08:36
01:10:56
09 May 2022
RF20
02:31:50
03:13:16
03:21:46
03:30:57
05:34:04
06:18:01
06:26:08
06:31:12
06:44:53
10 May 2022
RF21
22:46:25
23:17:30
23:37:26
23:52:47
01:53:34
11 May 2022
RF22
03:40:38
03:44:55
04:19:32
04:34:18
06:28:12
06:42:49
07:14:49
07:29:10
07:34:46
07:39:04
Altitude [km]
Temperature [°C]
RH [%]
Wind Speed [m/s]
Vertical Wind [m/s]

7 Appendix A: Listing of all sounding

#	Research Flight	Sounding	Drop point	Latitude [°]	Longitude [°]	Altitude [km]	Fall rate [m/s]
1	RF01	20220404_204346	SX CUYAMA	34.89998	-119.59804	3.4	-11.4
2	RF01	20220404_205320	SX 2	34.55605	-119.60918	3.4	-10.2
3	RF01	20220404_212424	SX 7	34.29454	-120.47984	3.4	-11.5
4	RF01	20220404_213400	SX 8	34.24931	-120.11994	3.3	-11.3
5	RF01	20220404_214517	SX 9	34.24933	-119.64223	3.4	-11.4
6	RF02	20220405_004532	SX 2	34.51015	-119.60963	3.5	-10.5
7	RF02	20220405_011806	SX 7	34.24948	-120.47802	3.4	-11.5
8	RF02	20220405_012736	SX 8	34.25002	-120.08018	3.4	-11.7
9	RF02	20220405_013810	SX 9	34.24956	-119.60973	3.4	-12.3
10	RF02	20220405_024822	SX 2	34.55970	-119.60609	3.4	-12.5
11	RF02	20220405_032951	SX 7	34.23775	-120.44847	3.4	-12.1
12	RF02	20220405_033810	SX 8	34.25021	-120.07883	3.5	-11.1
13	RF02	20220405_034824	SX 9	34.24992	-119.60874	3.5	-12.6
14	RF03	20220406_021832	SX CUYAMA	34.92094	-119.61083	3.5	-11.6
15	RF03	20220406_023043	SX 2	34.50962	-119.60990	3.5	-12.3
16	RF03	20220406_025235	SX 8	34.24959	-120.07905	3.4	-12.0
17	RF03	20220406_030413	SX 9	34.25113	-119.60958	3.5	-12.7
18	RF03b	20220406_063210	SX 2	34.51690	-119.64634	3.5	-13.6
19	RF03b	20220406_064337	SX 10	34.58984	-120.08080	3.5	-11.6
20	RF03b	20220406_065247	SX 8	34.24904	-120.08027	3.5	-11.4
21	RF03b	20220406_070446	SX 9	34.24968	-119.60895	3.5	-11.9
22	RF03b	20220406_072714	SX CUYAMA	34.92041	-119.60974	3.5	-12.6
23	RF04	20220413_200637	SX 2	34.51095	-119.61053	3.3	-11.0
24	RF04	20220413_204134	SX 4	34.84878	-120.20744	3.3	-12.7
25	RF04	20220413_210633	SX 7	34.24955	-120.47994	3.3	-11.4
26	RF04	20220413_211501	SX 8	34.25020	-120.07940	3.3	-11.8
27	RF04	20220413_212802	SX 9	34.25090	-119.60854	3.3	-11.8
28	RF05	20220414_004844	SX 2	34.53444	-119.60963	3.3	-12.4
29	RF05	20220414_013420	SX 7	34.24947	-120.48003	3.3	-11.9
30	RF05	20220414_014250	SX 8	34.25025	-120.08022	3.3	-11.3
31	RF05	20220414_015207	SX 9	34.25074	-119.60886	3.3	-11.5
32	RF05	20220414_025633	SX 2	34.52235	-119.60759	3.4	-12.4
33	RF05	20220414_033949	SX 7	34.24942	-120.47977	3.3	-12.1
34	RF05	20220414_034822	SX 8	34.25007	-120.07979	3.3	-11.4
35	RF05	20220414_035814	SX 9	34.25123	-119.60635	3.3	-10.9
36	RF06	20220417_195816	SX 2	34.51131	-119.60880	3.4	-12.8
37	RF06	20220417_202326	SX 4	34.85029	-120.21067	3.4	-11.6
38	RF06	20220417_205244	SX 7	34.24942	-120.47963	3.3	-13.5
39	RF06	20220417_210205	SX 8	34.25024	-120.07907	3.3	-12.0

#	Research Flight	Sounding	Drop point	Latitude [°]	Longitude [°]	Altitude [km]	Fall rate [m/s]
40	RF06	20220417_211234	SX 9	34.25209	-119.60841	3.3	-11.7
41	RF07	20220418_004316	SX 2	34.51096	-119.61047	3.4	-12.2
42	RF07	20220418_012327	SX 7	34.24937	-120.47830	3.4	-12.9
43	RF07	20220418_013215	SX 8	34.25026	-120.07951	3.4	-13.3
44	RF07	20220418_014210	SX 9	34.25073	-119.60831	3.4	-12.2
45	RF07	20220418_024338	SX 2	34.51048	-119.61018	3.4	-12.2
46	RF07	20220418_032334	SX 7	34.24963	-120.48049	3.4	-12.1
47	RF07	20220418_033201	SX 8	34.25020	-120.07957	3.4	-12.6
48	RF07	20220418_034129	SX 9	34.25061	-119.60854	3.4	-13.4
49	RF08	20220418_195747	SX 2	34.51045	-119.61029	3.4	-12.1
50	RF08	20220418_203315	SX 4	34.84894	-120.20979	3.4	-11.1
51	RF08	20220418_205217	SX 11	34.24968	-120.20969	3.4	-13.3
52	RF08	20220418_205854	SX 12	34.25009	-119.91010	3.4	-13.0
53	RF08	20220418_210414	SX 9	34.25025	-119.60976	3.4	-13.2
54	RF09	20220419_011202	SX 2	34.51031	-119.61095	3.4	-11.6
55	RF09	20220419_015244	SX 11	34.25000	-120.20944	3.4	-12.9
56	RF09	20220419_020120	SX 12	34.25042	-119.91037	3.4	-11.3
57	RF09	20220419_020644	SX 9	34.25053	-119.60924	3.4	-12.9
58	RF09	20220419_035825	SX 2	34.51115	-119.61022	3.4	-11.2
59	RF09	20220419_043904	SX 11	34.24984	-120.20989	3.4	-13.6
60	RF09	20220419_044704	SX 12	34.25030	-119.90974	3.4	-12.7
61	RF09	20220419_045215	SX 9	34.25065	-119.60973	3.4	-11.6
62	RF09	20220419_050348	SX 2	34.50996	-119.61082	3.4	-11.9
63	RF10	20220423_220139	SX CUYAMA	34.91906	-119.60927	3.3	-12.0
64	RF10	20220423_221328	SX 2	34.50835	-119.61038	3.3	-11.5
65	RF10	20220423_224114	SX 11	34.24991	-120.20952	3.3	-12.2
66	RF10	20220423_225012	SX 12	34.25029	-119.90995	3.4	-13.2
67	RF10	20220423_225659	SX 9	34.25021	-119.60848	3.3	-12.3
68	RF10	20220423_231002	SX 2	34.50970	-119.60979	2.4	-12.0
69	RF10	20220424_003622	SX 2	34.50632	-119.60691	2.4	-10.6
70	RF11	20220424_022439	SX 2	34.51022	-119.61077	3.4	-12.4
71	RF11	20220424_030216	SX 12	34.25028	-119.90980	3.4	-13.2
72	RF11	20220424_030906	SX 9	34.25085	-119.60972	3.4	-12.4
73	RF11	20220424_045515	SX 2	34.50951	-119.61175	3.4	-12.3
74	RF11	20220424_052106	SX 11	34.24862	-120.20918	3.4	-10.2
75	RF11	20220424_053016	SX 12	34.25035	-119.90960	3.4	-13.3
76	RF11	20220424_053709	SX 9	34.25080	-119.60852	3.4	-11.4
77	RF11	20220424_054835	SX 2	34.51097	-119.60988	3.4	-12.5
78	RF12	20220425_215404	SX CUYAMA	34.92118	-119.61037	3.4	-12.8
79	RF12	20220425_220633	SX 2	34.50956	-119.60984	3.4	-13.5

#	Research Flight	Sounding	Drop point	Latitude [°]	Longitude [°]	Altitude [km]	Fall rate [m/s]
80	RF12	20220425_223550	SX 11	34.24948	-120.20976	3.4	-13.3
81	RF12	20220425_224524	SX 12	34.25015	-119.90919	3.4	-11.8
82	RF12	20220425_225144	SX 9	34.25031	-119.60940	3.4	-11.5
83	RF12	20220426_003544	SX 2	34.50937	-119.61000	2.8	-12.2
84	RF13	20220426_022258	SX 2	34.51078	-119.61040	3.4	-12.7
85	RF13	20220426_025317	SX 11	34.24965	-120.20960	3.4	-13.2
86	RF13	20220426_030202	SX 12	34.25030	-119.90915	3.4	-13.6
87	RF13	20220426_030824	SX 9	34.24991	-119.60983	3.4	-11.7
88	RF13	20220426_045443	SX 2	34.50984	-119.61046	3.4	-12.6
89	RF13	20220426_052350	SX 11	34.24894	-120.20904	3.4	-11.6
90	RF13	20220426_053230	SX 12	34.25015	-119.90966	3.4	-13.1
91	RF13	20220426_053848	SX 9	34.25048	-119.60962	3.4	-13.7
92	RF13	20220426_054804	SX 2	34.51073	-119.61049	3.4	-11.9
93	RF14	20220428_214804	SX 2	34.51018	-119.61038	3.3	-11.4
94	RF14	20220428_222057	SX 4	34.85070	-120.20979	3.3	-14.1
95	RF14	20220428_223842	SX 11	34.24888	-120.20968	3.3	-11.5
96	RF14	20220428_224654	SX 12	34.25019	-119.90929	3.3	-13.6
97	RF14	20220428_225312	SX 9	34.25035	-119.60944	3.3	-12.9
98	RF14	20220429_003417	SX 2	34.51036	-119.61027	2.4	-11.3
99	RF15	20220429_021421	SX 2	34.51072	-119.60999	3.3	-12.2
100	RF15	20220429_025357	SX 12	34.25032	-119.89897	3.4	-12.4
101	RF15	20220429_030022	SX 9	34.25063	-119.61463	3.4	-13.2
102	RF15	20220429_044856	SX 2	34.50988	-119.61134	3.4	-12.4
103	RF15	20220429_051632	SX 11	34.24967	-120.20927	3.4	-11.7
104	RF15	20220429_052558	SX 12	34.25037	-119.90892	3.4	-12.2
105	RF15	20220429_053310	SX 9	34.25102	-119.60903	3.4	-11.2
106	RF15	20220429_054451	SX 2	34.50972	-119.60983	3.4	-13.2
107	RF16	20220504_195810	SX 2	34.51067	-119.61074	3.4	-13.6
108	RF16	20220504_202454	SX 4	34.84990	-120.21041	3.4	-13.1
109	RF16	20220504_204440	SX 11	34.24945	-120.20976	3.4	-13.0
110	RF16	20220504_205420	SX 12	34.25038	-119.90973	3.4	-13.3
111	RF16	20220504_210138	SX 9	34.25006	-119.60912	3.4	-12.2
112	RF16	20220504_225107	SX 2	34.50976	-119.60828	2.8	-12.3
113	RF17	20220505_005717	SX 2	34.51072	-119.61021	3.4	-13.6
114	RF17	20220505_012702	SX 11	34.24964	-120.20975	3.4	-11.8
115	RF17	20220505_013649	SX 12	34.25029	-119.90964	3.4	-13.6
116	RF17	20220505_014351	SX 9	34.25020	-119.60817	3.4	-13.3
117	RF17	20220505_033833	SX 2	34.51006	-119.61136	3.4	-13.3
118	RF17	20220505_040628	SX 11	34.24973	-120.20992	3.4	-13.6
119	RF17	20220505_041538	SX 12	34.25011	-119.90936	3.4	-13.0

#	Research Flight	Sounding	Drop point	Latitude [°]	Longitude [°]	Altitude [km]	Fall rate [m/s]
120	RF17	20220505_042231	SX 9	34.25011	-119.60899	3.4	-11.9
121	RF17	20220505_043208	SX 2	34.51146	-119.61015	3.4	-12.2
122	RF18	20220508_013736	SX 11	34.25066	-120.21041	2.5	-11.3
123	RF18	20220508_023019	SX 4	34.85095	-120.21104	2.4	-12.2
124	RF18	20220508_031553	SX 12	34.25504	-119.95032	3.4	-13.1
125	RF18	20220508_041552	SX 9	34.25066	-119.64991	3.4	-13.6
126	RF18	20220508_041940	SX 1	34.37077	-119.65128	3.4	-13.2
127	RF18	20220508_042418	SX 2	34.51044	-119.64957	3.4	-12.4
128	RF18	20220508_043854	SX CUYAMA	34.91887	-119.60979	3.4	-12.9
129	RF19	20220508_215035	SX 2	34.51031	-119.61056	3.4	-11.7
130	RF19	20220508_222551	SX 4	34.85046	-120.20945	3.4	-11.3
131	RF19	20220508_224630	SX 11	34.24952	-120.21024	3.3	-12.2
132	RF19	20220508_225418	SX 12	34.25014	-119.90556	3.4	-12.3
133	RF19	20220508_230021	SX 9	34.24110	-119.58527	3.4	-11.4
134	RF19	20220508_230836	SX 9	34.24797	-119.60841	2.4	-13.0
135	RF19	20220509_011056	SX 2	34.51014	-119.60983	3.0	-11.7
136	RF20	20220509_023150	SX 2	34.51030	-119.61017	3.4	-12.3
137	RF20	20220509_031316	SX 11	34.24975	-120.20982	3.3	-11.3
138	RF20	20220509_032146	SX 12	34.25005	-119.90933	3.3	-11.0
139	RF20	20220509_033057	SX 9	34.25150	-119.61023	3.3	-11.9
140	RF20	20220509_053404	SX 2	34.51033	-119.60999	3.4	-11.9
141	RF20	20220509_061801	SX 11	34.23544	-120.20887	3.4	-11.3
142	RF20	20220509_062608	SX 12	34.25018	-119.90813	3.4	-11.4
143	RF20	20220509_063112	SX 9	34.25022	-119.60910	3.4	-11.3
144	RF20	20220509_064453	SX 2	34.51059	-119.61010	3.4	-11.7
145	RF21	20220510_224625	SX 2	34.51062	-119.60970	3.3	-12.0
146	RF21	20220510_231730	SX 4	34.85020	-120.21027	3.3	-10.6
147	RF21	20220510_233726	SX 11	34.24923	-120.21060	3.3	-11.2
148	RF21	20220510_235247	SX 9	34.25005	-119.60766	3.3	-11.1
149	RF21	20220511_015334	SX 2	34.51057	-119.61025	2.4	-11.5
150	RF22	20220511_034038	SX 1	34.37076	-119.60835	3.3	-11.4
151	RF22	20220511_034455	SX 2	34.51176	-119.61100	3.3	-11.5
152	RF22	20220511_041932	SX 11	34.24905	-120.20985	3.3	-11.3
153	RF22	20220511_043418	SX 9	34.25008	-119.60930	3.3	-11.7
154	RF22	20220511_062812	SX 1	34.37047	-119.60971	2.4	-10.9
155	RF22	20220511_064249	SX 2	34.50995	-119.61091	3.3	-11.7
156	RF22	20220511_071449	SX 11	34.24909	-120.20995	3.3	-12.2
157	RF22	20220511_072910	SX 9	34.24992	-119.60892	3.3	-11.1
158	RF22	20220511_073446	SX 1	34.37035	-119.61037	3.3	-10.3
159	RF22	20220511_073904	SX 2	34.51102	-119.61023	3.3	-12.0

8 References

Vömel, H., I. Suhr, and G. Granger, 2019, NCAR/EOL/ISF Dropsonde NetCDF Data Files, UCAR/NCAR - Earth Observing Laboratory. https://doi.org/10.26023/54wh-rj45

Vömel, H., Goodstein, M., Tudor, L., Witte, J., Fuchs-Stone, Ž., Sentić, S., Raymond, D., Martinez-Claros, J., Juračić, A., Maithel, V., and Whitaker, J. W.: High-resolution in situ observations of atmospheric thermodynamics using dropsondes during the Organization of Tropical East Pacific Convection (OTREC) field campaign , Earth Syst. Sci. Data, 13, 1107–1117, https://doi.org/10.5194/essd-13-1107-2021, 2021

Wang, J., Bian, J., Brown, W. O., Cole, H., Grubišić, V., and Young, K.: Vertical Air Motion from T-REX Radiosonde and Dropsonde Data, J. Atmos. Ocean. Tech., 26, 928–942, https://doi.org/10.1175/2008JTECHA1240.1, 2009.